Stereochemistry of the Brivaracetam Diastereoisomers

Shi Qiu,[a] Kourosch Abbaspour Tehrani,[a] Sergey Sergeyev,[a] Patrick Bultinck, [b] Wouter Herrebout,*[a] and Benoit Mathieu [c]

Abstract: The stereochemistry of all four stereoisomers of brivaracetam is determined using vibrational circular dichroism (VCD) spectroscopy. By comparing experimentally obtained VCD spectra and computationally simulated ones, the absolute configurations can be confidently assigned without prior knowledge of their relative stereochemistry. Neither the corrected mean absolute errors analysis of the nuclear magnetic resonance (NMR) data, nor the matching of experimental and calculated infrared spectra allowed the diastereoisomers to be distinguished. VCD spectroscopy itself suffices to establish the absolute configurations of all diastereoisomers.

The relative stereochemistry could also be statistically confirmed by matching experimental and computed NMR spectra using the CP3 algorithm. The combination of VCD and NMR is recommended for molecules bearing more than one chiral center, as the relative configurations obtained from NMR serve as an independent check for those established with VCD. Analysis of the calculated VCD spectra reveals that the localized NH_2 scissoring mode at around 1600 cm^{-1} may be characteristic of intramolecular hydrogen bonding, and the orientation of the ethyl group is reflected by the delocalized modes between 1150 and 1050 cm^{-1}.

Keywords: Vibrational Circular Dichroism (VCD), Marker Bonds, Intramolecular Hydrogen Bond, Similarity Indices, Randomization plot

Introduction

Brivaracetam (UCB 34714, Scheme 1) or (2S)-2-[(4R)-2-oxo-4-propylpyrrolidin-1-yl] butanamide is a novel high-affinity synaptic vesicle protein 2A ligand [1] discovered and developed by UCB. With two chiral centers, 4 different diastereomers are possible that will henceforth all be referred to as brivaracetam diastereomers. According to regulatory agencies, such as the US FDA [2], stereoisomers for new pharmaceutical compounds should be separately assessed for their biological activities. To do so, all four stereoisomers of brivaracetam have been synthesized for analytical reference and testing purposes.

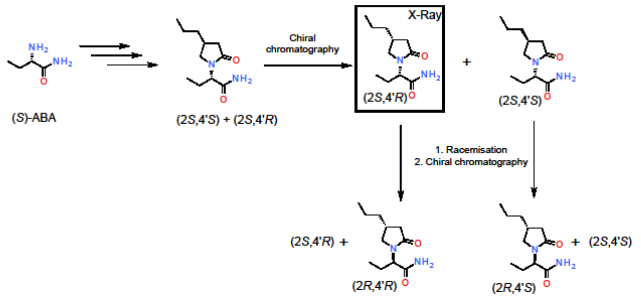

SCHEME 1 Synthetic routes to four stereoisomers of brivaracetam

Understanding the chiral structure and function is not only driven by legislative bodies but also a key step to recognize the role of chirality in chemical and biological processes. To meet this need, a reliable and streamlined approach for absolute configuration (AC) determinations of chiral molecules is of prime importance. VCD is an IR absorption-based chiroptical method capable of determining the AC of organic compounds [3], offering many advantages over other methods widely used since there is no need of either single crystals (for single crystal X-ray diffraction [4], derivatizations (as for NMR studies with e.g., chiral complexing agents) [5] nor the presence of chromophores as required for electronic circular dichroism [6]. Furthermore, VCD has the extra benefit of providing a detailed conformational analysis in solution. The method became much more popular when algorithms [7] appeared that allowed the interpretation of the spectra through comparison with theoretically obtained ones [8]. The number of applications of VCD for the determination of the AC of diastereoisomers increases every year [9-29], and in many cases the relative stereochemistry is already known. The purpose of the present paper was to use VCD to determine the ACs of all stereoisomers of brivaracetam with no prior knowledge of their relative stereochemistry. Using all four stereoisomers, experimental and theoretical spectra were

[a] *Dr. S. Qiu, Prof. dr. K.A. Tehrani, Dr. S. Sergueev, Prof. dr. W. Herrebout*
Department of Chemistry
University of Antwerp
Groenenborgerlaan 171, 2020 Antwerp, Belgium
Fax: (+)32650233
E-mail: wouter.herrebout@uantwerpen.be

[b] *Prof. dr. P. Bultinck*
Department of Inorganic and Physical Chemistry
Ghent University
Krijgslaan 281-S3, 9000 Ghent, Belgium

[c] *Dr. B. Mathieu*
UCB Pharma
1420 Braine-L'Alleud, Belgium

Received: ((will be filled in by the editorial staff))
Revised: ((will be filled in by the editorial staff))
Published online: ((will be filled in by the editorial staff))

obtained. Although the AC for each stereoisomer was known to UCB, the study proceeded blind as the four samples were anonymized. Knowledge of the AC was only used afterwards to establish whether or not VCD did suffice for a complete AC assignment of all four samples. Besides VCD, NMR spectra were also used to confirm the relative stereochemistry with the aid of statistical analyses.

Materials and Methods

STEREOSPECIFIC SYNTHESIS

Chiral assignment of the four isomers relied on the AC knowledge of starting chiral reagent S-ABA and the X-ray structure of brivaracetam, the latter providing the relative stereo information between position 2 and 4' chiral centers (see Figure 1 for atom numbering) [30]. With these two pieces of information, it was possible to unambiguously assign position 4'. 2R isomers were synthesized from the corresponding 2S by epimerization in basic conditions followed by a chiral separation step (Scheme 1). The pairs of enantiomers (2S,4'R)-(2R,4'S) and (2S,4'S)-(2R,4'R) shared the same AC independent spectroscopic data (NMR and IR, see later) and the same magnitude of the optical rotation, albeit with inverted sign ($[\alpha]_d^{20}$: -60(1)° and +59(1)° for (2S, 4'R) and (2R,4'S) and -47(1)° and +48(1)° for (2S,4'S) and (2R,4'R). The four experimental samples, each corresponding to a stereoisomer, were made available by UCB, Belgium with chemical and chiral purity ≥98 % (HPLC-UV) but without information on their stereochemistry, and were used without further purification.

IR AND VCD MEASUREMENTS

IR and VCD spectra were recorded on a BioTools dual-photo-elastic modulator (PEM) ChiralIR-2X spectrometer. The optimal frequency for the PEMs was set to 1400 cm^{-1}, and a resolution of 4 cm^{-1} was used throughout. A liquid cell equipped with BaF_2 windows with a path length of 100 µm was used. For all experiments, solutions of 7.0 mg in 0.1 mL of $CDCl_3$ were investigated. The solution spectra were recorded for 20000 scans. Based on the equality of the IR spectra for enantiomers and using the mirror image relationship between the VCD spectra, the enantiomeric pairs could easily be established within the four samples. For each enantiomeric pair, baseline corrections were introduced using the spectrum of a virtual racemate.

NMR SPECTROSCOPY

^1H, ^{13}C, COSY, NOESY, HMQC, DEPT, and HMBC were recorded at 400 MHz (^1H) and 100 MHz (^{13}C) using $CDCl_3$ as solvent and TMS as internal standard. Using the NMR and VCD data reported in the results, the following NMR characteristics could eventually be linked to the sets of enantiomers:

(2S, 4'R)-I and (2R, 4'S)-II: ^1H NMR ($CDCl_3$) δH 6.12 (s, 1H, NH), 5.26 (s, 1H, NH), 4.43 (dd, 1H, J=8.4, 7.2 Hz, C_2H), 3.49 (dd, 1H, J=9.6, 8.0 Hz, $C_{5'}H$), 3.00 (dd, 1H, J=9.7, 7.0 Hz, $C_{5'}H$), 2.59 (dd, 1H, J=16.8, 8.6 Hz, $C_{3'}H$), 2.34 (m, 1H, $C_{4'}H$), 2.08 (dd, 1H, J=16.8, 7.9 Hz, $C_{3'}H$), 1.95 (m, 1H, C_3-H), 1.69 (m, 1H, C_3-H), 1.22-1.48 (m, 4H, $C_{1''}H_2$ downfield and $C_{2''}$-H_2 upfield), 0.917 (t, 3H, $C_{3''}H_3$) , 0.913 (t, 3H, C_4-H_3); ^{13}C NMR ($CDCl_3$) δc 175.7 ($C_{2'}$), 171.9 (C_1), 56.1 (C_2), 49.6 ($C_{5'}$), 37.9 ($C_{3'}$), 36.7 ($C_{1''}$), 31.9 ($C_{4'}$), 20.8 (C_3), 20.5 ($C_{2''}$),14.0 ($C_{3''}$), 10.5 (C_4).

(2R, 4'R)-III and (2S, 4'S)-IV : ^1H NMR ($CDCl_3$) δH 6.17 (s, 1H, NH), 5.36 (s, 1H, NH), 4.44 (dd, 1H, J=8.9, 6.8 Hz, C_2H), 3.54 (dd, 1H, J=9.7, 7.9 Hz, $C_{5'}H$), 3.01 (dd, 1H, J=9.8, 6.6 Hz, $C_{5'}H$), 2.53 (dd, 1H, J=16.6, 8.5 Hz, $C_{3'}H$), 2.35 (m, 1H, $C_{4'}H$), 2.14 (dd, 1H, J=16.6, 7.8 Hz, $C_{3'}H$), 1.97 (m, 1H, C_3-H), 1.68 (m, 1H, C_3-H), 1.22-1.48 (m, 4H, $C_{1''}H_2$ downfield and $C_{2''}$-H_2 upfield), 0.926 (t, 3H, $C_{3''}H_3$) , 0.915 (t, 3H, C_4-H_3); ^{13}C NMR ($CDCl_3$) δc 175.5 ($C_{2'}$), 172.2 (C_1), 56.1 (C_2), 49.7 ($C_{5'}$), 37.7 ($C_{3'}$), 36.9 ($C_{1''}$), 31.8 ($C_{4'}$), 20.9 (C_3), 20.6 ($C_{2''}$),14.0 ($C_{3''}$), 10.5 (C_4).

COMPUTATIONAL METHODS

VCD spectra for diastereomers most often differ significantly, hence the possibility of using VCD as a technique to establish ACs. Moreover, there is a simple mirror image relationship between the geometries and chiroptical spectra of enantiomers. Experimental VCD spectra are not easily interpreted so quantum chemically calculated spectra for a set of chosen configurations are computed, although it suffices to compute only one representative of each enantiomeric pair as the spectrum of one enantiomer is simply the mirror image of that of the other. The geometry of enantiomers also exhibits mirror image symmetry so for each enantiomeric pair it also suffices to perform geometry optimizations for only one enantiomer. In this work, geometry optimizations were performed and spectral properties calculated for the (2R,4'S) and (2R,4'R) diastereoisomers. Through comparison with the experimental samples, we then aimed to establish which sample corresponds to which diastereomer. To obtain good starting points for ab initio geometry optimizations for the minima on the potential-energy surface, extensive conformational searching was performed at the molecular mechanics level using the MMFF94 [31], Sybyl [32], and MMFF94S [33] molecular mechanics force fields, as implemented in the Spartan08 [34] and Conflex [35-37] software packages using the Monte Carlo and reservoir-filling algorithms, respectively. Subsequently, the minima were further optimized at the density functional theory level using Gaussian 09 [38]. For each stationary point, the Hessian was diagonalized to establish that it corresponded to a minimum. Boltzmann populations, required to calculate Boltzmann weighed spectra, were derived from the relative enthalpies of the conformations studied using a temperature of 298 K and a pressure of 1 atm.

IR and VCD spectra were computed at the self-consistent reaction field (SCRF)-B3LYP/6-31G(d) level of theory, with SCRF [39] referring to the integral equation formalism model used to account for solute−solvent interactions, using a dielectric constant for chloroform of ε=4.71. The B3LYP functional is a commonly used functional for VCD calculations [3]. To allow comparison with experimental data, Lorentzian broadening was applied using a full width at half maximum of 10 cm^{-1}.

NMR shielding constants were computed using two different approaches [25]. The first is based on the use of linear regression data as suggested by Tantillo and co-workers [40,41]. This entails geometry optimizations at the B3LYP/6-31+G(d,p) level in the gas phase, and followed by computing the NMR shielding constants by the gauge including atomic orbital method

at the SCRF-mPW1PW91/6-311+G(2d,p) level using the implicit solvent model (chloroform, ε=4.71) (SCRF-mPW1PW91/6-311+G(2d,p)//B3LYP/6-31+G(d,p), Level A). Shielding constants relating to the hydrogen atoms in the methyl group were averaged. NMR chemical shifts relative to TMS were obtained applying linear regression parameters, notably for ^{1}H data, the slope and intercept used were set to -1.0936 and 31.8018, respectively, while for the ^{13}C data values of -1.0533 and 186.5242 were used in the formulae in the Cheshire database [42].

The other method, futher annotated as Level B, does not rely on database parameters [25] Geometry optimization and calculations of the NMR shielding constants were performed at the SCRF-mPW1PW91/6-311+G(2d,p) level (chloroform, ε=4.71) for all conformations. NMR chemical shifts relative to TMS were obtained applying linear regression between computed isotropic shielding constants of both (2R,4'S) and (2R,4'R) and experimental chemical shifts of both experimental samples II and III. For ^{1}H data, the slope and intercept obtained here were -0.99303 and 31.8481, respectively, while for the ^{13}C data values of 1.0255 and 186.2902 were used. A tight correlation is indicated by the high R^2 values of 0.9968 and 0.9998 for ^{1}H and ^{13}C data, respectively.

Henceforth, computationally generated spectra will be referred to by the AC they reflect: (2R,4'S) and (2R,4'R) in this case. Experimental samples are referred to with Roman numerals I-IV and from the moment theory and experiment can be matched, this is reflected in a notation such as (2R,4'S)-II and (2R,4'R)-III meaning, for example, that experimental sample II contains, according to the computed spectra, AC (2R,4'S).

Results and Discussion

First, the results of the conformational analysis are presented followed by the results of the use of IR and VCD to assign the absolute configuration. NMR is then used to check the relative configurations. Finally the VCD spectrum-structure relationship is explored.

CONFORMATIONAL ANALYSIS

The molecular mechanics search yielded 189 and 198 conformers for the (2R,4'S) and (2R,4'R) diastereoisomers, respectively. These geometries were further optimized at different levels of theory for the IR, VCD, and NMR calculations (see computational methods), respectively. The key structural difference among these conformers lies in the torsion angles of τ_1, τ_2, τ_3, and τ_4 (Figure 1), and the puckering of the γ-lactam. At the SCRF-B3LYP/6-31G(d) level, the four most abundant conformers of each diastereoisomer (Figure 2) are characterized by either $\tau_1 \approx 83°$ for (2R,4'S) or $\tau_1 \approx 88°$ for (2R,4'R) and $\tau_2 \approx -77°$, each one stabilized by two cooperative intramolecular hydrogen bonds NH···O and C(2)H···O.

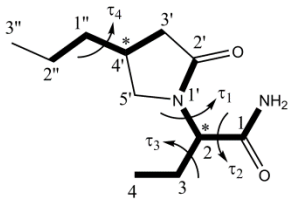

FIGURE 1 Structure of brivaracetam and atom numbering. Brivaracetam has two chiral centers, C_2 and $C_{4'}$, and thus has four stereoisomers

INFRARED SPECTROSCOPY

In Figure 3, the experimental IR spectra of the four samples are compared to the calculated ones of (2R,4'S) and (2R,4'R) at the SCRF-B3LYP/6-31G(d) level of theory. As IR spectra for enantiomers are the same, assignments are made down to the level of enantiomeric pairs. Careful inspection of the experimental data obtained for the different samples shows that subtle changes in relative intensities, band widths, and overlap can be detected for a variety of spectral regions including that of, amongst others, the NH_2 scissoring mode and the C-H bending vibrations in the γ-lactam ring and the propyl group. The subtle differences in the experimental data allow identification of the samples to the two families of enantiomers present, but they are too small to confidently assign their relative stereochemistry.

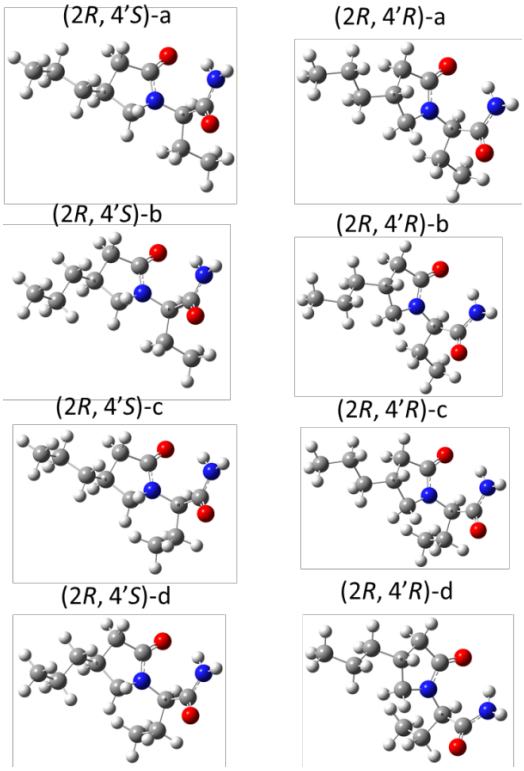

FIGURE 2. Optimized lowest-energy conformers of (2R,4'S) and (2R,4'R) at the SCRF-B3LYP/6-31G(d) level of theory. The Boltzmann populations of the conformations a-d shown are summarized in Tables 4 and 5.

To ensure that the visual interpretation was not subject to human bias, the CompareVOA algorithm [43] based on neighborhood similarity [44-47] was used to evaluate the IR similarity (Table 1). The calculated IR spectra were scaled to compensate for the overestimation of the vibrational frequencies in the harmonic approximation. This scale factor is chosen such that the calculated IR spectrum gives the largest similarity to the experimental one. The calculated spectrum of (2R,4'S) gives an IR similarity (Σ(IR)) of roughly 89% with the experimental data for all samples, and similarly the calculated spectrum of (2R,4'R) gives Σ(IR) equal to roughly 92% with the experimental data for all samples. The IR similarity is high in all cases, indicating that in this case IR spectra do not suffice for distinguishing between diastereoisomers.

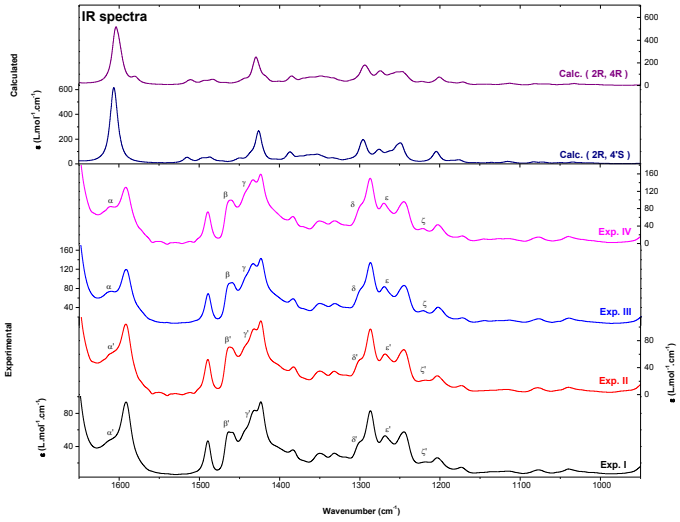

FIGURE 3. Calculated SCRF-B3LYP/6-31G(d) IR spectra of (2R, 4'S) and (2R, 4'R) (upper panel) and experimental IR spectra of the four samples (lower panel). Subtle changes due to differences in relative stereochemistry observed in the experimental spectra are indicated by Greek symbols.

ASSIGNING THE ABSOLUTE CONFIGURATIONS : VCD SPECTROSCOPY

The experimental VCD spectra of the four samples were compared to the calculated ones of (2R, 4'S) and (2R, 4'R) at the SCRF-B3LYP/6-31G(d) level of theory (Figure 4).

Inspection of the experimental VCD spectra shows that the four samples are clearly separated into two enantiomeric pairs ([I, II] and [III, IV]) based on the mirror-image relationship. Comparing the spectra of sample II and (2R, 4'S), and of sample III and (2R, 4'R), good agreement is found in which all intense VCD peaks are correctly predicted in the region of 1600–1000 cm^{-1}. Two features are used to distinguish between the two diastereoisomers. First, in the region of 1500–1400 cm^{-1}, the peaks 3, 4 and 5 in III show an intense triplet that is reproduced only by the spectrum of (2R,4'R). These transitions involve mainly CH_2 wagging, C-N stretching of the γ-lactam ring, and C(2)-H bending at one of the chiral centers. The other feature concerns the signs of peaks 8 and 12. These characteristic peaks are both positive in II, while peak 8 is positive and 12 is negative in III. These features are well reproduced by the spectra of (2R, 4'S) and (2R, 4'R), respectively. The vibration associated with peak 8 is related to CH bending at the two chiral centers and CH_2 wagging of the two CH_2 groups adjacent to the chiral centers, i.e. C(3')H_2 and C(5')H_2. The vibration related to peak 12 mainly involves C(4')H bending, C(3')H_2 and C(5')H_2 wagging of the γ-lactam ring. These important differences, together with the enantiomeric relationship, lead to the conclusion that I corresponds to the (2S,4'R) AC, II is (2R,4'S), III is (2R,4'R), and IV corresponds to (2S,4'S).

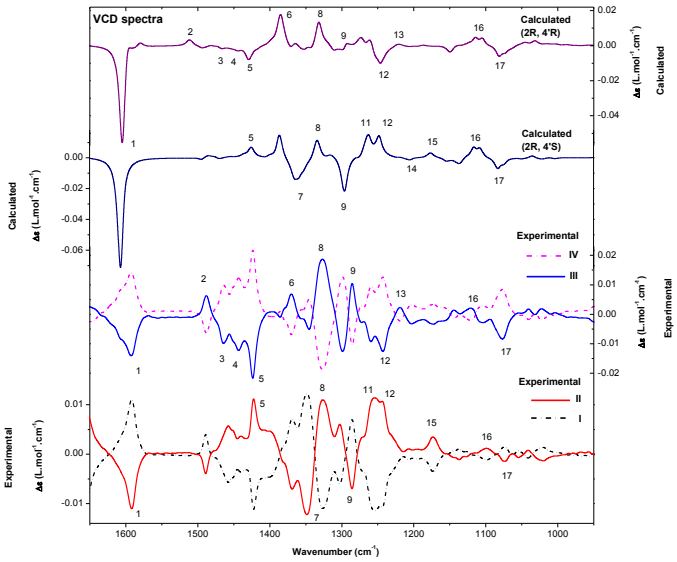

FIGURE 4 Calculated SCRF-B3LYP/6-31G(d) VCD spectra of (2R, 4'S) and (2R, 4'R) (upper two traces) and experimental VCD spectra of the four samples (I, II, III and IV, lower). Important similarity features are numbered.

To further assess the reliability of the AC assignment, the CompareVOA algorithm was used to evaluate the VCD similarity, and the statistical significance [48] of the VCD similarity was validated using a randomization test (Table 1). The calculated VCD spectra were scaled using the same scale factors used for IR spectra. Single VCD similarity (Σ(VCD)) has a value between 0 and 100 %, and gives the similarity between the calculated and experimental VCD spectra. The enantiomeric similarity index Δ gives the difference between the values of Σ(VCD) for both enantiomers of a given diastereoisomer. Σ(VCD) and Δ are then compared to a database of previous validated assignments to get a confidence level. Alternatively, to evaluate the robustness of the VCD similarity independent of any previous databases, a measure based on a randomization test was used. Similarities of IR and VCD ($R^{(VCD)}_{calc,\exp}$) are first calculated based on neighbourhood similarity, although here the similarity between the experimental and calculated or random spectra is computed as a signed quantity (see ref. 48 for details). Then, random VCD spectra x are generated by placing bands with random signs and intensities to get statistically random similarities $R^{(VCD)}_{x,\exp}$. The significance statistic P obtained from the randomization plot gives the probability that the VCD similarity cannot be improved by a random VCD spectrum, i.e. P [$R^{(VCD)}_{x,\exp} < |R^{(VCD)}_{calc,\exp}|$]. So the P value indicates whether the numerical degree of VCD similarity is significant, and can be used to evaluate the robustness of VCD similarity [48]. Put simply, P measures the probability that by using a random spectrum, one could come to a good assignment that, however, bears no chemical

significance. For the pair (I, II), the results shown in Table 1 indicate good agreement between II and (2R,4'S) with large values of Σ(VCD) and Δ, whereas no good agreement is found for (2R,4'R) or its enantiomer (2S,4'S). To establish the significance of the VCD similarity, 25000 random spectra were generated by placing bands with random signs, intensities, and frequencies in the region of 1550–950 cm^{-1} for II. The randomization plot shows a tight distribution for II versus (2R,4'S) (Figure 5a). The red dot at the top right labels the actual VCD similarity with the original computed VCD spectrum. The P-value (99.66%) indicates that there is only a 0.34% chance of randomly generating a better VCD spectrum than the original computed spectrum. For II and (2R,4'R), or alternatively, I and (2S,4'S), however, the randomization plot (Figure 5b) exhibits a relatively circular distribution of the data points with many randomly generated VCD spectra having a higher similarity with respect to the experimental value. Moreover, the negative slope indicates that II would correspond more to (2S,4'S) although the similarity would still be far smaller compared to that in Figure 5a. The CompareVOA results and the P value thus both support the manual assignment of AC.

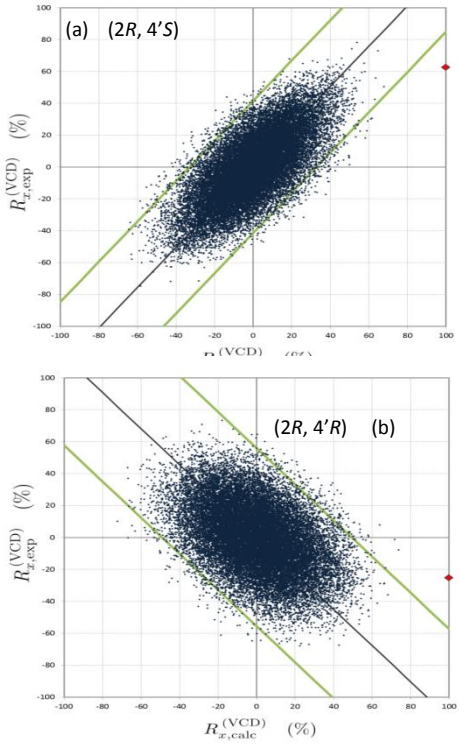

FIGURE 5 $R_{x,\mathrm{exp}}^{(VCD)}$ versus $R_{x,calc}^{(VCD)}$ scatter diagram for II and (2R,4'S) (a), and (2R,4'R) (b) at the SCRF-B3LYP/6-31G(d) level. For the scatter diagram, blue data points represent random spectra. The red data point represents the raw calculated spectrum and a similarity of $R_{calc,\mathrm{exp}}^{(VCD)}$ with respect to the experiment. The black line is obtained by orthogonal regression. The area between the parallel green lines contains 99% of the blue data points.

CONFIRMING THE RELATIVE STEREOCHEMISTRY : NMR SPECTROSCOPY

NMR is arguably one of the most widespread spectroscopic techniques, and although without special, and often cumbersome, provisions, it does not allow distinction of enantiomers, but it is one of the most often used and best techniques for distinguishing diastereomers. Therefore, it is appropriate to validate the assignment based on VCD, although only down to the level of the relative configuration. To that end, the experimental 1H and 13C chemical shifts were manually assigned based on 1H, 13C, COSY, NOESY, HMQC, HMBC, and DEPT NMR data, and computed NMR shifts were utilized in assigning the relative stereochemistry.

NMR calculations were performed at two levels of theory: SCRF-mPW1PW91/6-311+G(2d,p)//B3LYP/6-31+G(d,p) suggested by Tantillo and co-workers,31,32 and SCRF-mPW1PW91/6-311+G(2d,p)//idem. Idem denotes the use of the same level of theory for the geometry optimization and the calculation of expectation values, while SCRF-mPW1PW91/6-311+G(2d,p)//B3LYP/6-31+G(d,p) reflects the use of B3LYP/6-31+G(d,p) for geometry optimization, and SCRF-mPW1PW91/6-311+G(2d,p) for the calculation of the NMR data (and possibly other expectation values) using the B3LYP/6-31+G(d,p) geometry. The scaled NMR chemical shifts from linear regression with isotropic shielding constants calculated at the SCRF-mPW1PW91/6-311+G(2d,p)//idem level are shown in Figure 6 along with the experimental data.

TABLE 1. Numerical Comparison Describing the Similarity Between the Calculated VCD Spectra for Stereoisomers at the SCRF-B3LYP/6-31G(d) level and the Experimental VCD Spectra for Samples I, II, III, and IV. All Samples were Obtained Using the 950−1550 cm^{-1} Spectral Range

Calculated	Numerical comparison	Experimental			
		I	**II**	**III**	**IV**
(2*R*,4'*S*)	[a]σ	0.976	0.976	0.977	0.977
	[b]∑(IR) (%)	89.3	89.3	89.1	89.1
	[c]∑(VCD)	[g]-	68.9	-	43.8
	[d]Δ (%)	-	58.0	-	16.4
	[e]CL (%)	-	99	-	65
	[f]*P*	-	99.66	-	49.96
(2*R*,4'*R*)	σ	0.974	0.974	0.974	0.974
	∑(IR) (%)	91.6	91.6	91.6	91.6
	∑(VCD)	49.5	-	69.5	-
	Δ(%)	22.4	-	60.9	-
	CL (%)	62	-	99	-
	P	77.40	-	99.88	-

[a]σ: scaling factor. [b]∑ (IR): IR similarity from CompareVOA. [c]∑ (VCD): single VCD similarity from CompareVOA, gives the similarity between the calculated and experimental VCD spectra. [d]Δ: enantiomeric similarity index from CompareVOA, gives the difference between the values of ∑(VCD) for both enantiomers of a given diastereoisomer. [e]CL: confidence level from CompareVOA. [f]P: significance statistic P from the randomization plot gives the probability that the VCD similarity cannot be improved by a random VCD spectrum. [g]Dashes represent negative Δ values which mean that the agreement for the given stereostructure is smaller than its mirror image.

Table 2 shows a summary of the corrected mean absolute errors (CMAE) [49,50] and the largest deviation (Δδ) comparing the computed data to experimental ones at the two calculation levels. It is clear that, based on the values CMAE and Δδ, the scaled NMR chemical shifts from linear regression with fully ab initio calculation results at Level B fitted experimental data better than the SCRF-mPW1PW91/6-311+G(2d,p) // B3LYP/6-31+G(d,p) Level A values. However, both the CMAE and Δδ values are similar for the two diastereoisomers, and thus the relative stereochemistry cannot be properly established using CMAE and Δδ.

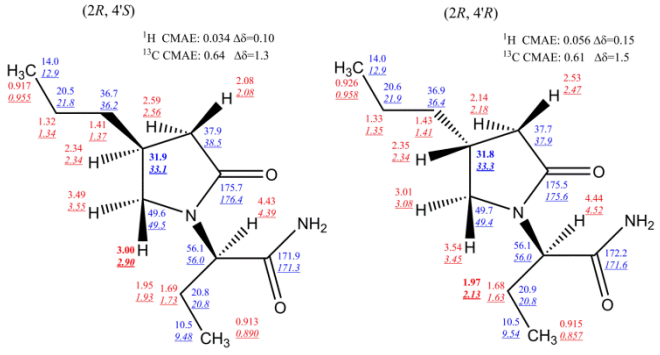

FIGURE 6 Computed H (red) and C (blue) chemical shifts (ppm, relative to TMS) at the SCRF-mPW1PW91/6-311+G(2d,p)//idem level (Level B) compared to the experimental ones for (2*R*,4'*S*) and (2*R*,4'*R*). Experimental shifts are in normal text and computed shifts are in underlined italics. CMAE=corrected mean absolute error, computed as $(1/n)\sum_i^n|\delta_{cal}- \delta_{exp}|$,where δ_{cal} refers to the scaled calculated chemical shifts. Δδ:largest deviations, and are highlighted in bold text for each set of data.

TABLE 2. CMAEs and Largest Deviations for Comparison of Calculated NMR Chemical Shifts at the Two Levels of SCRF-mPW1PW91/6-311+G(2d,p) // B3LYP/6-31+G(d,p) (Level A) and SCRF-mPW1PW91/6-311+ G(2d,p) // idem (Level B) for Each Diastereoisomer with Relative Configuration to the Experimental Data for Samples II and III

			Level A		Level B	
			(2*R*, 4'*S*)	(2*R*, 4'*R*)	(2*R*, 4'*S*)	(2*R*, 4'*R*)
II	^{13}C	CMAE[a] (ppm)	1.1	1.3	0.64	0.53
		Δδ[b] (ppm)	2.7	2.9	1.3	1.5
	^{1}H	CMAE (ppm)	0.13	0.11	0.034	0.067
		Δδ (ppm)	0.36	0.46	0.10	0.17
III	^{13}C	CMAE (ppm)	1.2	1.3	0.76	0.61
		Δδ (ppm)	3.0	3.0	1.3	1.5
	^{1}H	CMAE (ppm)	0.14	0.12	0.041	0.056
		Δδ (ppm)	0.37	0.48	0.11	0.15

[a]CMAE: corrected mean absolute error, computed as $(1/n)\sum_i^n|\delta_{cal}- \delta_{exp}|$,where δ_{cal} refers to the scaled calculated chemical shifts. [b]Δδ: largest deviations.

Table 3 reports the results of the CP3 [51] analysis, showing the quantifiable confidence comparing the calculated data to the experimental data at the two levels. The CP3 statistical analysis is applied to assign the relative configurations of diastereoisomers when both experimental data sets are available. At Level B, the CP3 data according to the VCD results, for the correct assignment (II=(2R,4'S) & III=(2R,4'R)) are 0.46, -0.03, and 0.22 for respectively ^{13}C individually, ^{1}H individually, and both data sets together, and, according to the VCD results, for the wrong assignment (II=(2R,4'R) & III=(2R,4'S)) are -1.50, -1.66 and -1.58 for respectively ^{13}C individually, ^{1}H individually, and both data sets together. This leads to a 100.0 % probability for the right assignment in all the cases. The CP3 values for the calculations using Level A reflect the same conclusion. The CP3 statistical results indicate a relative configuration assignment (2R,4'S)-I (or II) and (2R,4'R)-III (or IV) from the VCD spectra. Moreover, in this case CP3 performs better than CMAE in distinguishing between diastereoisomers.

TABLE 3. CP3 Results for the Comparison of the Calculated NMR Chemical Shifts at the SCRF-mPW1PW91/6-311+G(2d,p) // B3LYP/6-31+G(d,p) and SCRF-mPW1PW91/6-311+G(2d,p) // idem for Each Diastereoisomer with Relative Configuration to the Experimental Data for Samples II and III

		Level A [a]		Level B [a]	
		II= (2*R*, 4'*S*) III= (2*R*, 4'*R*)	II= (2*R*, 4'*R*) III= (2*R*, 4'*S*)	II= (2*R*, 4'*S*) III= (2*R*, 4'*R*)	I= (2*R*, 4'*R*) III= (2*R*, 4'*S*)
CP3	^{13}C	0.37	-1.97	0.46	-1.50
	^{1}H	0.11	-1.25	-0.03	-1.66
	^{13}C and ^{1}H	0.24	-1.61	0.22	-1.58
Probability (%)	^{13}C	100.0	0.0	100.0	0.0
	^{1}H	100.0	0.0	100.0	0.0
	^{13}C and ^{1}H	100.0	0.0	100.0	0.0

[a] Level A: SCRF-mPW1PW91/6-311+G(2d,p) // B3LYP/6-31+G(d,p); Level B: SCRF-mPW1PW91/6-311+G(2d,p) // idem

VCD MARKER OF INTRAMOLECULAR HYDROGEN BONDS

The high sensitivity of VCD spectroscopy to subtle structural changes stimulated us to conduct an extensive study of the spectrum-structure relationship. Conformers with a Boltzmann population over 1% and the calculated VCD spectra at the level of SCRF-B3LYP/6-31G(d) are thus classified into categories according to their structural differences (Tables 4 and 5, and Figure 7).

For (2R,4'S), the eight lowest-energy conformers have an exo conformation (ring down-puckered with respect to the amide group) with $\tau_1 \approx 83°$ and $\tau_2 \approx -77°$, each one being stabilized by two cooperative intramolecular hydrogen bonds NH···O and

C(2)H···O. This group of conformations is defined as category A. In category B, four conformers have an endo conformation (ring up-puckered with respect to the amide group) with $\tau_1 \approx 88°$ and $\tau_2 \approx -77°$ or -74°, each one stabilized by two cooperative intramolecular hydrogen bonds NH···O and C(2)H···O as well. In category C, four conformers have also endo conformation, albeit with "abnormal" $\tau_1 \approx -75°$ and $\tau_2 \approx 54°$ or 60°, that is, each conformer is stabilized by two cooperative intramolecular hydrogen bonds NH···O and C(3)H···O instead of C(2)H···O. In each category, the ethyl (τ_3) and the propyl (τ_4) substituents have two stable orientations.

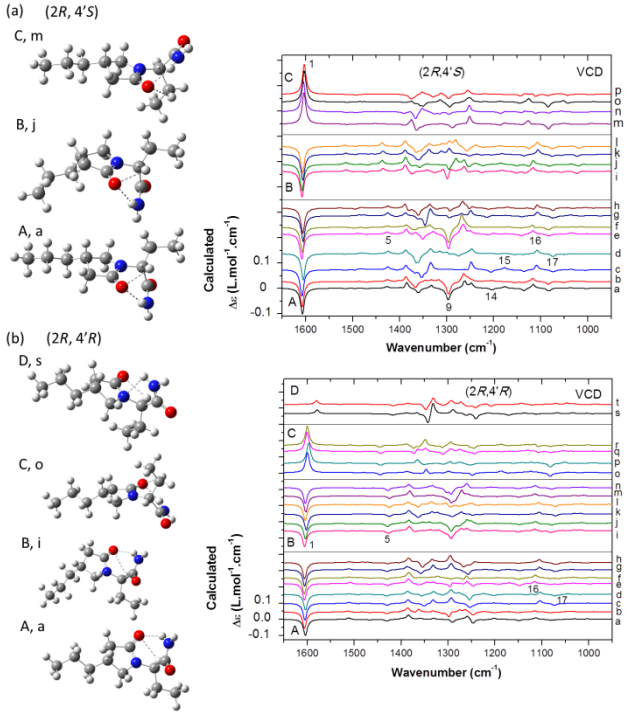

FIGURE 7 Calculated VCD spectra of individual conformers of (a) (2R,4'S) and (b) (2R,4'R) with a Boltzmann population over 1% at the level of SCRF-B3LYP/6-31G(d). The categories shown are obtained by analyzing the occurrence of possible intramolecular hydrogen bonds and by studying the puckering of the γ-lactam. For each category, a representative geometry is also given.

Comparison of the VCD spectra in the three categories shows that

i) the "abnormal" dihedral angles τ_1 and τ_2 in category C reverse the VCD sign of peak 1 that corresponds to NH_2 scissoring

ii) the endo conformation in category B blue shifts peak 5 by roughly 10 cm^{-1} relative to category A, but keeps the positive VCD signal. Category C further shifts it roughly 14 cm^{-1} to higher wavenumbers relative to category B, while the VCD signal is extremely weak. The corresponding vibrational transition involves C(5')H_2 wagging and C-N stretching of the γ-lactam ring, and C(2)-H bending

iii) the strong negative VCD peak 9 is dominated by the conformers with $\tau_3 \approx -69°$ (conformers a, b, e, f, i and j), and the vibrational transition mainly involves C(3)H_2 twisting, NH bending, C(2)H bending, and CH_2 wagging

iv) peaks 16 and 17 are more sensitive to τ_3: change of τ_3 either induces wavenumber shifts of the double positive-negative VCD couplets 16 and 17 in categories A and B, or alters the VCD pattern in category C. The transition of peak 16 represents mainly NH_2 rocking, C(2)-C(3) stretching, C(3)H_2 and C(4)H_3 wagging, and C(3')H_2 twisting; and the transition of 17 involves NH_2 rocking, C(4)H bending, C(3)H_2 twisting, and C(4)H_3 wagging

v) weak peaks 14 and 15 appear to be more sensitive to τ_4 in category A and C, change of τ_4 induces variation of the VCD pattern in this region. Peak 14 involves C(2)H bending, C(2)-N stretching, and C(3')H_2 twisting; and the transition of peak 15 is more localized on the two CH_2 twisting of the γ-lactam ring

TABLE 4. Structural Parameters of Conformers of (2*R*,4'*S*) with a Boltzmann Fraction (Bf) Over 1% at the SCRF-B3LYP/6-31G(d) Level

		Bf	Rotatable bonds (degrees)				Bond distance (Å)
		(%)	τ_1	τ_2	τ_3	τ_4	
A	a	18.3	83.0	-77.5	-69.5	65.6	NH···O(2'): 2.121 C(2)H···O(2'): 2.463
	b	14.9	83.1	-77.9	-69.3	178	NH···O(2'): 2.132 C(2)H···O(2'): 2.461
	c	12.7	83.8	-76.6	-175	65.7	N-H···O(2'): 2.152 C2-H···O(2'): 2.444
	d	11.7	83.9	-76.0	-175	178	NH···O(2'): 2.143 C(2)H···O(2'): 2.444
	e	3.70	87.7	-78.3	-69.3	63.4	NH···O(2'): 2.129 C(2)H···O(2'): 2.463
	f	3.43	83.1	-77.9	-69.6	180	NH···O(2'): 2.133 C(2)H···O(2'): 2.456
	g	2.96	84.0	-76.5	-176	64.0	NH···O(2'): 2.159 C(2)H···O(2'): 2.442
	h	2.68	83.8	-77.2	-176	180	NH···O(2'): 2.159 C(2)H···O(2'): 2.441
B	i	2.26	87.5	-77.4	-68.0	173	NH···O(2'): 2.165 C(2)H···O(2'): 2.446
	j	2.26	87.5	-76.7	-67.9	70.1	NH···O(2'): 2.155 C(2)H···O(2'): 2.451
	k	1.66	88.7	-74.4	-172	173	NH···O(2'): 2.199 C(2)H···O(2'): 2.433
	l	1.54	88.5	-74.6	-172	70.5	NH···O(2'): 2.192 C(2)H···O(2'): 2.436
C	m	2.63	-74.7	54.1	-169	65.5	NH···O(2'): 1.914 C(2)H···O(2'): 3.985 C(3)H···O(2): 2.538
	n	2.41	-74.7	59.9	-56.8	65.2	NH…O(2'): 1.903 C(2)H···O(2'): 3.989 C(3)H···O(2): 2.539
	o	2.34	-74.6	53.8	-169	178	NH···O(2'): 1.912 C(2)H···O(2'): 3.984 C(3)H···O(2): 2.532
	p	2.20	-74.9	60.1	-57.0	178	NH···O(2'): 1.905 C(2)H···O(2'): 3.988 C3-H···O(1):2.537

For (2R,4'R), the eight lowest-energy conformers in category A have endo conformation with $\tau_1 \approx 88°$ and $\tau_2 \approx -77°$ or -76°, each one being stabilized by two cooperative intramolecular hydrogen bonds NH···O and C(2)H···O. In category B, the six confomers have exo conformation with $\tau_1 \approx 84°$ or 83° and $\tau 2 \approx -77°$ or -78°, each one also being stabilized by two cooperative intramolecular hydrogen bonds NH···O and C(2)H···O as well. In category C, the four conformers have an exo conformation, with "abnormal" $\tau_1 \approx -71°$ and $\tau_2 \approx 55°$, 56° or 61°, however. As a consequence, each conformer is stabilized by two cooperative intramolecular hydrogen bonds NH···O and C(3)H···O. In category D, the two conformers have endo conformation, with "abnormal" $\tau_1 \approx 121°$ and $\tau_2 \approx -23°$ or -24°, however. Consequently, each conformer is stabilized by two cooperative intramolecular hydrogen bonds C(2)H···O and NH···N. In each category, the propyl and ethyl substituents both have two stable orientations. Comparison of the VCD spectra in the four categories shows that

i) the "abnormal" dihedral angles τ_1 and τ_2 in categories C and D reverse the VCD sign of peak 1, the vibrational motion of which is NH_2 scissoring. The formation of the NH···N in category D makes a red-shift of roughly 20 cm^{-1} compared to the conformers in category C

ii) the "abnormal" τ_1 and τ_2 in category C blue shifts peak 5 by approximately 14 cm^{-1} relative to categories A and B, while in category D the peak has a red shift of approximately 12 cm^{-1} compared to categories A and B. Interestingly, this peak has a consistent negative VCD sign in all categories. The vibrational transition corresponding to peak 5 involves C(5')H_2 wagging and C-N stretching of the γ-lactam ring, and C(2)-H bending

iii) Similarly to (2R,4'S), peaks 16 and 17 are more sensitive to τ_3: change of τ_3 either induces the wavenumber shifts of the double positive-negative VCD couplets 16 and 17 in categories A and B, or alters the VCD pattern in category C. The transition of peak 16 represents mainly NH_2 rocking, C(2)-C(3) stretching, C(3)H_2 and C(4)H_3 wagging and C(3')H_2 twisting, and the transition of 17 involves NH_2 rocking, C(4)H bending, C(3)H_2 twisting, and C(4)H_3 wagging.

For both (2R,4'S) and (2R,4'R), the localized NH_2 scissoring mode (peak 1) near 1600 cm^{-1} reverses its VCD sign when the intramolecular hydrogen bonds NH···O and C(2)H···O are replaced by C(3)H···O or NH···N, while the latter two can be distinguished by the VCD wavenumber shifts and intensities. Such a localized mode may be used as a marker to identify the intramolecular hydrogen bonds. Moreover, the VCD shifts of peak 5 also indicate the change of the intramolecular hydrogen bonds, and the transition mode of peak 5 is ascribed as C(5')H_2 wagging and C-N stretching of the γ-lactam ring, and C(2)-H bending. Finally, the delocalized modes between 1150 and 1050 cm^{-1} (peaks 16 and 17) reflect the orientation of the ethyl group.

TABLE 5. Structural Parameters of Conformers of (2*R*,4'*R*) with a Boltzmann Fraction Over 1% at the SCRF-B3LYP/6-31G(d) Level

		Bf (%)	Rotatable bonds (degrees)				Bond distance (Å)
			τ_1	τ_2	τ_3	τ_4	
A	a	12.8	87.7	-77.4	-68.0	-65.5	NH…O(2'): 2.149 C(2)H…O(2'): 2.456
	b	11.7	87.8	-77.3	-68.2	-177	NH…O(2'): 2.151 C(2)H…O(2'): 2.453
	c	8.44	88.2	-75.7	-172	-65.5	NH…O(2'): 2.179 C(2)H…O(2'): 2.440
	d	7.44	88.7	-76.6	-173	-177	NH…O(2'): 2.199 C(2)H…O(2'): 2.434
	e	2.80	87.5	-77.4	-68.3	-63.7	N-H…O(2'): 2.145 C(2)H…O(2'): 2.454
	f	2.46	87.6	-77.8	-68.3	-179	NH…O(2'): 2.156 C(2)H…O(2'): 2.452
	g	1.77	88.3	-75.8	-172	-63.5	NH…O(2'): 2.183 C(2)H…O(2'): 2.440
	h	1.54	88.6	-75.7	-172	-179	NH…O(2'): 2.192 C(2)H…O(2'): 2.438
B	i	4.19	83.7	-77.3	-68.4	-172	NH…O(2'): 2.130 C(2)H…O(2'): 2.455
	j	4.06	83.2	-78.2	-69.3	-70.4	NH…O(2'): 2.136 C(2)H…O(2'): 2.454
	k	2.93	84.1	-77.0	-175	-173	NH…O(2'): 2.158 C(2)H…O(2'): 2.435
	l	2.77	83.9	-76.5	-175	-70.9	NH…O(2'): 2.156 C2-H…O(2'): 2.442
	m	1.04	82.8	-78.0	-69.3	-174	N-H…O(2'): 2.122 C2-H…O(2'): 2.463
	n	1.01	83.1	-78.1	-69.3	-68.2	N-H…O(2'): 2.129 C2-H…O(2'): 2.459
C	o	3.24	-70.5	54.9	-168	-65.5	N-H…O(2'): 1.923 C2-H…O(2'): 3.985 C3-H…O(2'): 2.529
	p	3.18	-70.7	56.0	-169	-178	N-H…O(2'): 1.926 C2-H…O(2'): 3.984 C3-H…O(2'): 2.525
	q	2.50	-70.7	60.8	-57.4	-178	N-H…O(2'): 1.921 C2-H…O(2'): 3.986 C3-H…O(2'): 2.531
	r	2.50	-70.6	60.5	-56.9	-66.0	N-H…O(2'): 1.922 C2-H…O(2'): 3.987 C3-H…O(2'): 2.531
D	s	4.48	121	-23.1	-171	-65.8	N-H…O(2'): 3.484 C2-H…O(2'): 2.354 N-H…N: 2.390
	t	4.09	122	-23.7	-171	-178	N-H…O(2'): 3.507 C2-H…O(2'): 2.354 N-H…N: 2.395

Bf: Boltzmann fraction based on relative enthalpies.

Conclusion

Vibrational circular dichroism (VCD) was used to assign the stereochemistry of all four stereoisomers of brivaracetam. Based on manual assignment and statistical analyses, the absolute configurations can be confidently assigned as (2S,4'R)-I, (2R,4'S)-II, (2R,4'R)-III and (2S,4'S)-IV without prior knowledge of their relative stereochemistry. The IR similarity is high between the calculated spectrum and the experimental spectrum of each diastereoisomer in both cases of comparison, and thus the IR spectra here can barely detect the relative configurations. Calculations of the NMR properties at the two levels of theory, aided by the CP3 statistical analysis, indicate that the relative configurations proposed by VCD spectra are very reliable, thus confirming the relative stereochemistry. The CMAE analysis cannot distinguish between the two diastereoisomers at either

level of theory. The combination of VCD and NMR is clearly the most powerful discriminatory method for diastereoisomers. The spectrum-structure analysis of the calculated VCD spectra shows that the localized NH_2 scissoring mode in the VCD spectra at ~1600 cm^{-1} may be used as a marker to identify the intramolecular hydrogen bonds, and the orientation of the ethyl group is reflected by the delocalized modes between 1150 and 1050 cm^{-1}. Confrontation of the spectroscopically obtained conclusions with that of single crystal X-ray diffraction, originally not disclosed, reveals that the spectroscopic assignment is correct. The spectroscopic data, however, also reveal useful information on the properties of the molecules in solution, a medium closer to the biologically relevant environment.

Acknowledgements

Financial support of the study and supply of original brivaracetam stereoisomers samples by UCB Pharma is acknowledged. Financial support through the Fund for Scientific Research (FWO - Vlaanderen), the Special Research Fund (BOF), and the Tech Transfer departments at the Universities of Ghent and Antwerp is acknowledged. The computational resources and services used in this work were provided by the VSC Flemish Supercomputing Centre. Financial support through the Hercules Foundation allowing the purchase of NMR equipment (AHUA13005)

REFERENCES AND NOTES

1. Van Paesschen W, Hirsch E, Johnson M, Falter U, von Rosenstiel, P. Efficacy and tolerability of adjunctive brivaracetam in adults with uncontrolled partial-onset seizures: A phase IIb, randomized, controlled trial. *Epilepsia* **2013**;54:89–97.

2. FDA'S policy statement for the development of new stereoisomeric drugs. *Chirality* **1992**;4:338–340.

3. Stephens PJ, Devlin FJ, Cheeseman J.R. *VCD spectroscopy for organic chemists*. New York: CRC Press; **2012**, p 370.

4. Flack, HD, Bernardinelli G. The use of X-ray crystallography to determine absolute configuration. *Chirality* **2008**;20:681–690.

5. Seco JM, Quiñoá E, Riguera R. Assignment of the absolute configuration of polyfunctional compounds by NMR using chiral derivatizing agents. *Chem. Rev.* **2012**;112:4603–4641.

6. Lightner DA, Gurst, JE. Organic conformational analysis and stereochemistry from circular dichroism spectroscopy, Wiley: New York, **2000**.

7. Stephens PJ. Theory of vibrational circular dichroism. *J. Phys. Chem.* **1985**;89:748–752.

8. He Y, Bo W, Dukor RK, Nafie LA. Determination of absolute configuration of chiral molecules using vibrational optical activity: a review. *Appl. Spectrosc.* **2011**;65:699–723.

9. Debie E, Kuppens T, Vandyck K, Van der EyckenJ, Van Der Veken B, Herrebout W, Bultinck P. Vibrational circular dichroism DFT study on bicyclo[3.3.0]octane derivatives. *Tetrahedron: Asymmetry* **2006**;17:3203–3218.

10. Muñoz MA, Muñoz O, Joseph-Nathan P. Absolute configuration of natural diastereoisomers of 6β-hydroxyhyoscyamine by vibrational circular dichroism. *J. Nat. Prod.* **2006**;*69*:1335–1340.

11. Bercion S, Buffeteau T, Lespade L, Martin M.-A.C.D. IR, VCD, 1H and 13C NMR experimental and theoretical studies of a natural guaianolide: Unambiguous determination of its absolute configuration. *J. Mol. Struct.* **2006**;791:186–192.

12. Muñoz MA, Chamy C, Carrasco A, Rovirosa J, San Martín A, Joseph-Nathan P. Diastereoisomeric assignment in a pacifenol derivative using vibrational circular dichroism. *Chirality* **2009**;21:E208–E214.

13. Batista Jr JM, Batista ANL, Rinaldo D, Vilegas W, Cass QB, Bolzani VS, Kato MJ, López SN, Furlan M, Nafie LA. Absolute configuration reassignment of two chromanes from Peperomia obtusifolia (piperaceae) using VCD and DFT calculations. *Tetrahedron: Asymmetry* **2010**;21:2402–2407.

14. Longhi G, Abbate S, Scafato P, Rosini C. A vibrational circular dichroism approach to the determination of the absolute configuration of flexible and transparent molecules: fluorenone ketals of 1,n-diols. *Phys. Chem. Chem. Phys.* **2010**;12:4725–4732.

15. Lattanzi A, Scettri A, Zanasi R, Devlin FJ, Stephens PJ. Absolute configuration assignment of norcamphor-derived furyl hydroperoxide using density functional theory calculations of optical rotation and vibrational circular dichroism. *J. Org. Chem.* **2010**;75:2179–2188.

16. Muñoz MA, Muñoz O, Joseph-Nathan P. Absolute configuration determination and conformational analysis of (−)-(3S,6S)-3α,6β-diacetoxytropane using vibrational circular dichroism and DFT techniques. *Chirality* **2010**;22:234–241.

17. Yang G, Tran H, Fan E, Shi W, Lowary TL, Xu Y. Determination of the absolute configurations of synthetic daunorubicin analogues using vibrational circular dichroism spectroscopy and density functional theory. *Chirality* **2010**;22: 734–743.

18. Cherblanc F, Lo Y-P, De Gussem E, Alcazar-Fuoli L, Bignell E, He Y, Chapman-Rothe N, Bultinck P, Herrebout WA., Brown R, Rzepa HS, Fuchter, MJ. On the determination of the stereochemistry of semisynthetic natural product analogues using chiroptical spectroscopy: desulfurization of epidithio-dioxopiperazine fungal metabolites. *Chem. Eur. J.* **2011**;17: 11868–11875.

19. Suárez-Castillo OR, Meléndez-Rodríguez M, Castelán-Duarte LE, Zúñiga-Estrada EA, Cruz-Borbolla J, Morales-Ríos MS, Joseph-Nathan P. Absolute configuration assignment of 3-oxindolylacetyl-4-phenyloxazolidinone derivatives. *Tetrahedron: Asymmetry* **2011**;22:2085–2098.

20. Manríquez-Torres JJ, Torres-Valencia JM, Gómez-Hurtado MA, Motilva V, García-Mauriño S, Ávila J, Talero E, Cerda-García-Rojas CM, Joseph-Nathan P. Absolute configuration of 7,8-seco-7,8-oxacassane diterpenoids from Acacia schaffneri. *J. Nat. Prod.* **2011**;74:1946–1951.

21. Gordillo-Román B, Camacho-Ruiz J, Bucio MA, Joseph-Nathan P. Chiral recognition of diastereomeric 6-cedrols by vibrational circular dichroism. *Chirality* **2012**;24:147–154.

22. Muñoz MA, Perez-Hernandez N, Pertino MW, Schmeda-Hirschmann G, Joseph-Nathan P. Absolute configuration and 1H NMR characterization of rosmaridiphenol diacetate. *J. Nat. Prod.* **2012**;75:779–783.

23. Felippe LG, Batista Jr JM, Baldoqui DC, Nascimento IR, Kato MJ, He Y, Nafie LA, Furlan M. VCD to determine absolute configuration of natural product molecules: secolignans from Peperomia blanda. *Org. Biomol. Chem.* **2012**;10:4208-4214.

24. De Gussem E, Bultinck P, Feledziak M, Marchand-Brynaert J, Stevens CV, Herrebout W. Vibrational circular dichroism versus optical rotation dispersion and electronic circular dichroism for diastereomers: the stereochemistry of 3-(1'-hydroxyethyl)-1-(3'-phenylpropanoyl)-azetidin-2-one. *Phys. Chem. Chem. Phys.* **2012**;14:8562–8571.

25. Qiu S, De Gussem E, Abbaspour Tehrani K, Sergeyev S, Bultinck P, Herrebout W. Stereochemistry of the tadalafil diastereoisomers: a critical assessment of vibrational circular dichroism, electronic circular dichroism, and optical rotatory dispersion. *J. Med. Chem.* **2013**;56:8903–8914.

26. Hopmann KH, Šebestík J, Novotná J, Stensen W, Urbanová M, Svenson J, Svendsen JS, Bouř P, Ruud K. Determining the absolute configuration of two marine compounds using vibrational chiroptical spectroscopy. *J. Org. Chem.* **2012**;77:858–869.

27. Li X, Hopmann KH, Hudecová J, Isaksson J, Novotná J, Stensen W, Andrushchenko V, Urbanová M, Svendsen J-S, Bouř P, Ruud K. Determination of absolute configuration and conformation of a cyclic dipeptide by NMR and chiral spectroscopic methods. *J. Phys. Chem. A* **2013**;117:1721–1736.

28. De Gussem E, Herrebout W, Specklin S, Meyer C, Cossy J, Bultinck P. Strength by joining methods: combining synthesis with NMR, IR, and vibrational circular dichroism spectroscopy for the determination of the relative configuration in hemicalide. *Chem. Eur. J.* **2014**;20:17385–17394.

29. Dezhahang Z, Poopari MR, Hernandez FE, Diaz C, Xu Y. Diastereomeric preference of a triply axial chiral binaphthyl based molecule: a concentration dependent study by chiroptical spectroscopies. *Phys. Chem. Chem. Phys*. **2014**;16:12959–12967.

30. Kenda BM, Matagne AC, Talaga PE, Pasau PM, Differding E, Lallemand BI, Frycia AM, Moureau FG Klitgaard HV, Gillard M R.; Fuks, B.; Michel, P. Discovery of 4-substituted pyrrolidone butanamides as new agents with significant antiepileptic activity. J. Med. Chem. 2004, 47, 530–549.

31. Halgren, TA. Merck molecular force field. I. Basis, form, scope, parameterization, and performance of MMFF94. *J. Comput. Chem.* **1996**;17:490–519.

32. Clark M, Cramer RD, Van Opdenbosch N. Validation of the general purpose tripos 5.2 force field. *J. Comput. Chem.* **1989**;10:982–1012.

33. Halgren TA. MMFF VII. Characterization of MMFF94, MMFF94s, and other widely available force fields for conformational energies and for intermolecular-interaction energies and geometries. *J. Comput. Chem.* **1999**;20:730–748.

34. Spartan'08. Wavefunction, Inc., 2008.

35. CONFLEX Program. Conflex Corporation, Tokyo.

36. Goto H, Osawa E. Corner flapping: a simple and fast algorithm for exhaustive generation of ring conformations. *J. Am. Chem. Soc.* **1989**;111:8950–8951.

37. Goto H, Osawa E. An efficient algorithm for searching low-energy conformers of cyclic and acyclic molecules. *J. Chem. Soc. Perkin Trans.* **1993**;20:187–198.

38. Frisch MJ, Trucks GW, Schlegel HB, Scuseria GE, Robb MA, Cheeseman JR, Scalmani G, Barone V, Mennucci B, Petersson GA, Nakatsuji H, Caricato M, Li X, Hratchian HP, Izmaylov AF, Bloino J, Zheng G, Sonnenberg JL, Hada M, Ehara M, Toyota K, Fukuda R, Hasegawa J, Ishida M, Nakajima T, Honda Y, Kitao O, Nakai H, Vreven T, Montgomery Jr. JA, Peralta JE, Ogliaro F, Bearpark M, Heyd JJ, Brothers E, Kudin KN, Staroverov VN, Kobayashi R, Normand J, Raghavachari K, Rendell A, Burant JC, Iyengar SS, Tomasi J, Cossi M, Rega N, Millam NJ, Klene M, Knox JE, Cross JB, Bakken V, Adamo C, Jaramillo J, Gomperts R, Stratmann RE, Yazyev O, Austin AJ, Cammi R, Pomelli C, Ochterski JW, Martin RL, Morokuma K, Zakrzewski VG, Voth GA, Salvador P, Dannenberg JJ, Dapprich S, Daniels AD, Farkas Ö, Foresman JB, Ortiz JV, Cioslowski J, Fox DJ. Gaussian 09 (Revision D.1). Gaussian, Inc., Wallingford CT, 2009.31. Lodewyk MW, Siebert MR, Tantillo DJ. Computational prediction of H-1 and C-13 chemical shifts: A useful tool for natural product, mechanistic, and synthetic organic chemistry. *Chem. Rev.* **2012**;112:1839–1862.

39. Scalmani G, Frisch MJ. Continuous surface charge polarizable continuum models of solvation. I. General formalism. *J. Chem. Phys.* **2010**;132:114110.

40. Lodewyk MW, Tantillo DJ Prediction of the structure of nobilisitine A using computed NMR chemical shifts. *J. Nat. Prod.* **2011**;74:1339–1343.

41.Tantillo DJ. Walking in the woods with quantum chemistry - applications of quantum chemical calculations in natural products research. *Nat. Prod. Rep.* **2013**;30:1079–1086.

42. Chemical Shift Repository for computed NMR scaling factors, http://cheshirenmr.info /.

43. Debie E, De Gussem E, Dukor RK, Herrebout W, Nafie LA, Bultinck P. A Confidence level algorithm for the determination of absolute configuration using vibrational circular dichroism or Raman optical activity. *ChemPhysChem* **2011**;12:1542-1549.

44. Kuppens T, Langenaeker W, Tollenaere JP, Bultinck P. Determination of the stereochemistry of 3-hydroxymethyl-2,3-dihydro-[1,4]dioxino[2,3-b]-pyridine by vibrational circular dichroism and the effect of DFT integration grids. *J. Phys. Chem. A* **2003**;107:542–553.

45. Kuppens, T.; Vandyck, K.; Van der Eycken, J.; Herrebout, W.; van der Veken, B. J.; Bultinck, P. Determination of the absolute configuration of three as-hydrindacene compounds by vibrational circular dichroism. J. Org. Chem. 2005, 70, 9103-9114.

46. Kuppens, T.; Vandyck, K.; van der Eycken, J.; Herrebout, W.; van der Veken, B.; Bultinck, P. A DFT conformational analysis and VCD study on methyl tetrahydrofuran-2-carboxylate. Spectrochimica Acta A 2007, 67, 402–411.

47. Kuppens, T. Determination of methodology to assign the absolute configuration using vibrational circular dichroism. PhD thesis, Ghent University (Belgium), 2006.

48. Vandenbussche J, Bultinck P, Przybył AK, Herrebout WA. Statistical validation of absolute configuration assignment in vibrational optical activity. *J. Chem. Theory Comput.* **2013**; 9:5504–5512.

49. Barone G, Gomez-Paloma L, Duca D, Silvestri A, Riccio R, Bifulco G. Structure validation of natural products by quantum-mechanical GIAO calculations of 13C NMR chemical shifts. *Chem. Eur. J.* **2002**;8:3233–3239.

50. Barone G, Duca D, Silvestri A, Gomez-Paloma L, Riccio R, Bifulco G. Determination of the relative stereochemistry of flexible organic compounds by ab initio methods: conformational analysis and Boltzmann-averaged GIAO 13C NMR chemical shifts. *Chem. Eur. J.* **2002**;8:3240–3245.

51. Smith SG, Goodman JM. Assigning the stereochemistry of pairs of diastereoisomers using GIAO NMR shift calculation. *J. Org. Chem.* **2009**;74:4597–4607.

Graphical Abstract